# DRP1-dependent mitochondrial fission initiates follicle cell differentiation during *Drosophila* oogenesis

Kasturi Mitra, Richa Rikhy, Mary Lilly, and Jennifer Lippincott-Schwartz

Cell Biology and Metabolism Program, Eunice Kennedy Shriver National Institute of Child Health and Human Development, National Institutes of Health, Bethesda, MD 20892

Exit from the cell cycle is essential for cells to initiate a terminal differentiation program during development, but what controls this transition is incompletely understood. In this paper, we demonstrate a regulatory link between mitochondrial fission activity and cell cycle exit in follicle cell layer development during *Drosophila melanogaster* oogenesis. Posterior-localized clonal cells in the follicle cell layer of developing ovarioles with down-regulated expression of the major mitochondrial fission protein DRP1 had mitochondrial elements extensively fused instead of being dispersed. These cells did not exit the cell cycle. Instead, they excessively proliferated, failed to activate Notch for differentiation, and exhibited downstream developmental defects. Reintroduction of mitochondrial fission activity or inhibition of the mitochondrial fusion protein Marf-1 in posterior-localized DRP1-null clones reversed the block in Notch-dependent differentiation. When DRP1-driven mitochondrial fission activity was unopposed by fusion activity in Marf-1–depleted clones, premature cell differentiation of follicle cells occurred in mitotic stages. Thus, DRP1-dependent mitochondrial fission activity is a novel regulator of the onset of follicle cell differentiation during *Drosophila* oogenesis.

## Introduction

Dynamic rearrangements of mitochondria, coordinated by the fission factor DRP1 (dynamin-related protein 1; Ingerman et al., 2005; Ishihara et al., 2009) and fusion factors MFN1 and MFN2 (mitofusins 1 and 2; Chen et al., 2003), are important for many physiological processes. These include apoptosis (Frank et al., 2001; Goyal et al., 2007), response to starvation (Gomes et al., 2011; Rambold et al., 2011), maintenance of mitochondrial DNA integrity (Chen et al., 2010), embryonic development (Chen et al., 2003; Ishihara et al., 2009), and mitochondrial quality control (Twig et al., 2008). Recently, mitochondrial fission/fusion dynamics have been linked to S-phase entry during cell cycle progression (Mitra et al., 2009), with levels of DRP1 regulated in a cell cycle–dependent manner (Taguchi et al., 2007; Horn et al., 2011). Whether such cell cycle control by mitochondria impacts the cell's decision to exit the cell cycle and enter a differentiation program in whole organisms remains unknown. Here, we manipulate key mitochondrial fission/fusion proteins in the epithelial follicle cell layer of *Drosophila melanogaster* egg chambers and perform live-cell imaging to visualize the relationship between mitochondrial dynamics and cell fate determination.

## Results and discussion

The *Drosophila* follicle cell layer encapsulates egg chambers containing 15 nurse cells and one oocyte (Fig. 1 A). The follicle cells comprising this cell layer progress through different developmental stages (Roth, 2001). During stages 1–5 (S1–5), most follicle cells undergo mitotic divisions, with a few cells exiting the mitotic cycle under Notch activation to form stalk cells separating consecutive egg chambers (Ruohola et al., 1991; de Cuevas et al., 1997). During S6–8, all follicle cells exit the mitotic cycle in response to Notch activation and differentiate into an endocycling, polarized epithelium patterned into posterior

K. Mitra and R. Rikhy contributed equally to this paper.

Correspondence to Jennifer Lippincott-Schwartz: lippincj@mail.nih.gov

Abbreviations used in this paper: AFC, anterior follicle cell; DN, dominant negative; EGFR, EGF receptor; FLIP, fluorescence loss in photobleaching; FLP, flippase; FRT, flip recombinase target; Hnt, Hindsight; MBC, main body cell; N-Act, activated Notch; NECD, Notch extracellular domain; NICD, Notch intracellular domain; PFC, posterior follicle cell; ROI, region of interest; TMRE, tetramethylrhodamine ethyl ester; tub, tubulin; UAS, upstream activation sequence; UbiGFP, ubiquitin promoter–GFP.



The Rockefeller University Press $30.00
J. Cell Biol. Vol. 197 No. 4 487–497
www.jcb.org/cgi/doi/10.1083/jcb.201110058

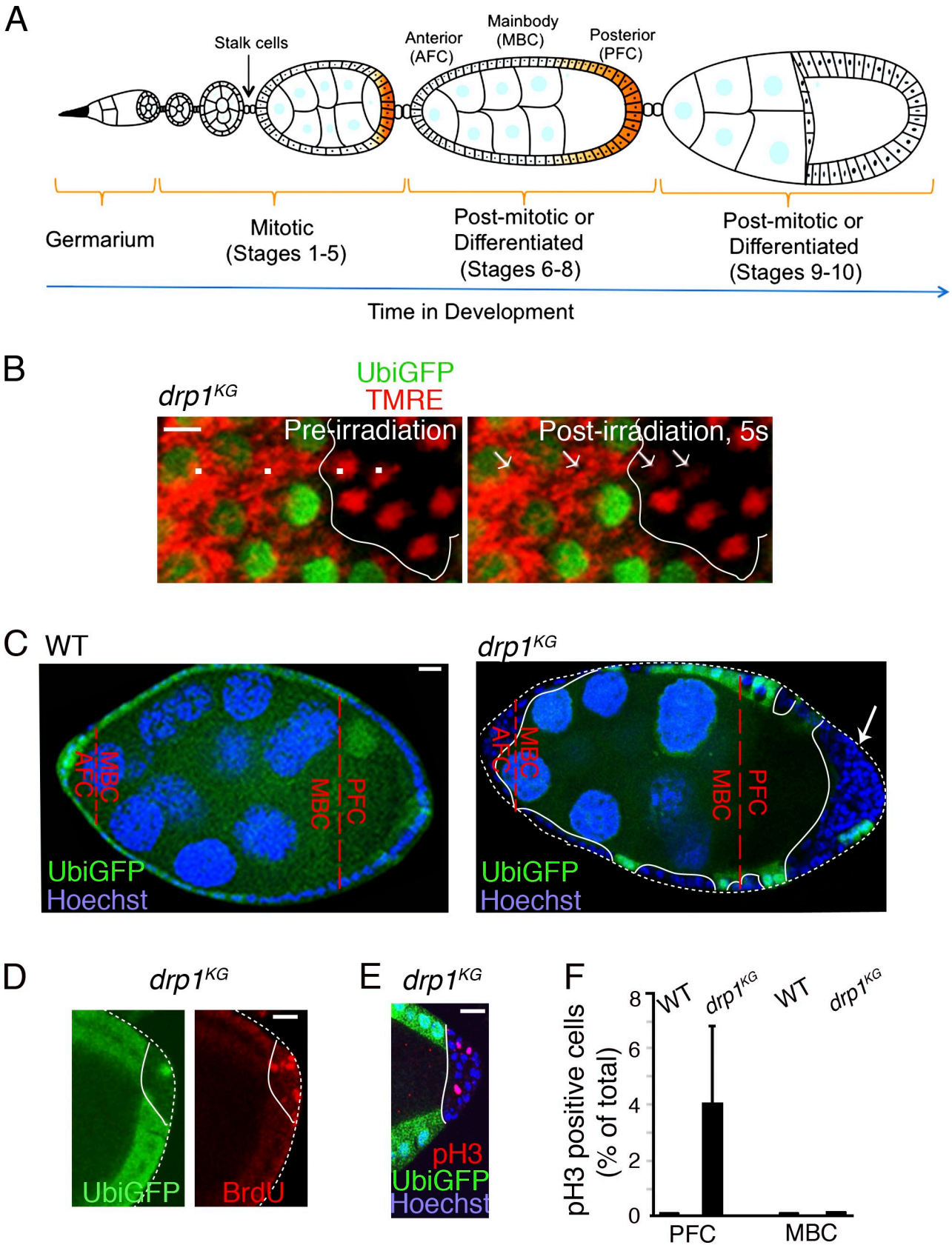


Figure 1. **DRP1 down-regulation inhibits mitochondrial fission and maintains proliferation in the postmitotic follicle cell layer.** (A) *Drosophila* follicle cell lineage during different developmental stages of the ovariole. (B, left) Microirradiation of TMRE-labeled mitochondria in nonclonal (containing UbiGFP) and *drp1*$^{KG}$ clones (lacking UbiGFP) was performed at white points. (right) This caused rapid loss of all TMRE signal only in *drp1*$^{KG}$ clones (with clustered mitochondria) after irradiation (arrows point to the effect on TMRE signal). (C) *drp1*$^{KG}$ clonal follicle cells in a S8 egg chamber. Nonclonal cells express UbiGFP, whereas *drp1*$^{KG}$ clones lack UbiGFP. Red lines demarcate the boundary between patterned zones. The arrow points to proliferating *drp1*$^{KG}$ PFC clones.

follicle cells (PFCs), main body cells (MBCs), and anterior follicle cells (AFCs; Van Buskirk and Schüpbach, 1999; van Eeden and St Johnston, 1999; López-Schier and St Johnston, 2001). To examine the effect of inhibiting mitochondrial fission activity in this system, we generated *Drosophila* follicle cell clones homozygous for a functionally null allele of DRP1 called *drp1*$^{KG}$ (see Materials and methods). Clones were identified by lack of a ubiquitin promoter–GFP (UbiGFP) label in their nucleus. The potentiometric dye tetramethylrhodamine ethyl ester (TMRE), which incorporates into the mitochondrial matrix, was used to label mitochondria (Mitra et al., 2009).

In an S10 egg chamber, nonclonal cells containing a nuclear UbiGFP label have mitochondrial elements widely distributed (Fig. 1 B). Microirradiation at a single point within mitochondria of these cells triggers depolarization (i.e., loss of TMRE signal) only at the irradiated site, with little loss of TMRE outside the microirradiated site (Fig. 1 B, postirradiation). This suggested the mitochondrial network of these cells is discontinuous. In *drp1*$^{KG}$ clones (no UbiGFP label), mitochondria were tightly clustered in a small region of each cell (Fig. 1 B). Single-point microirradiation of mitochondria in a *drp1*$^{KG}$ clone depolarizes the cell's entire mitochondrial cluster, with complete loss of TMRE signal in 5 s (Fig. 1 B, postirradiation). This indicated that mitochondria in *drp1*$^{KG}$ clones are highly fused. Reduced mitochondrial fission in *drp1*$^{KG}$ clones, therefore, causes normally fragmented mitochondrial elements in follicle cells to hyperfuse into a tight cluster.

We next examined whether the presence of *drp1*$^{KG}$ clones affects follicle epithelial layer organization. In S6–8 egg chambers, follicle cells normally form a single epithelial monolayer (Fig. 1 C, left). The presence of *drp1*$^{KG}$ clones, however, disrupts this monolayer arrangement (Fig. 1 C, right). The effect is most striking in the PFC region, in which *drp1*$^{KG}$ clones massively overproliferate (Fig. 1 C, arrow). The overpopulated clones undergo mitotic cycling even at S10 or later: they incorporate BrdU, demonstrating that they synthesize DNA (Fig. 1 D), and stain with pH3 antibody, indicating that they transit through mitosis (Fig. 1, E and F). Surrounding heterozygous tissue and *drp1*$^{KG}$ MBC clones, in contrast, are postmitotic: they neither incorporate BrdU (Fig. 1 D) nor stain for pH3 (Fig. 1, E and F). DRP1 depletion thus prevents cell cycle exit primarily in *drp1*$^{KG}$ PFC clones, leading to their overpopulation in postmitotic egg chambers.

As cell cycle exit is a prerequisite for initiating differentiation (Jasper et al., 2002), we examined whether the *drp1*$^{KG}$ PFCs are prevented from differentiating. Follicle cells in S6–8 egg chambers normally undergo cell cycle exit to differentiate under the influence of the homeodomain gene Hindsight (Hnt; Sun and Deng, 2007). Notably, clones of *drp1*$^{KG}$ in the PFC region marked by CD8GFP (see Materials and methods) fail to express Hnt, unlike surrounding nonclonal cells (Fig. 2 A, *drp1*$^{KG}$). 95% of *drp1*$^{KG}$ PFC clones show this phenotype ($n = 35$), whereas no *drp1*$^{KG}$ MBC clonal cells do (Fig. S1 A). Thus, *drp1*$^{KG}$ PFC clones fail to differentiate.

Hnt expression is rescued in all *drp1*$^{KG}$ PFC clones generated in the background of HA-DRP1 ($n = 35$; Fig. 2 A, *drp1*$^{KG}$ + HA-DRP1) and in 43% of *drp1*$^{KG}$ PFC clones with DRP1 reintroduced into them ($n = 32$; Fig. S1 B). In both conditions, DRP1 expression prevented the clustered mitochondrial phenotype (Fig. S1, C–D) characteristic of *drp1*$^{KG}$ clones (Fig. 2 B). Lack of differentiation in *drp1*$^{KG}$ PFC clones, therefore, results from loss of DRP1 activity.

Down-regulation of Marf-1, the *Drosophila* homologue of mitofusins (Deng et al., 2008), combined with DRP1 down-regulation in *drp1*$^{KG}$ PFC clones causes 22% of the clones to now partially express Hnt (Fig. 2 A, *drp1*$^{KG}$ + Marf-1 RNAi). Because Marf-1 RNAi expression causes mitochondrial fragmentation when expressed alone (Fig. 2 C, S8 MBCs; and Fig. S1 E, S10 MBCs) or in *drp1*$^{KG}$ PFC clones (Fig. S1 F), we concluded that fragmentation of mitochondria reverses the differentiation block in *drp1*$^{KG}$ PFCs. Therefore, DRP1-driven mitochondrial fission is required for PFCs to differentiate. Loss of function of the inner mitochondrial membrane fusion protein OPA1 caused cell death in this system (unpublished data).

Differentiation of *Drosophila* follicle cells requires Notch receptor activation (Ruohola et al., 1991; López-Schier and St Johnston, 2001). Upon ligand binding, the Notch receptor is cleaved to release the Notch intracellular domain (NICD), which redistributes into the nucleus to activate genes required for differentiation. To investigate whether DRP1-driven mitochondrial fission activity acts upstream or downstream of Notch activation in driving PFC differentiation, we examined whether NICD is cleaved and released from the plasma membrane in *drp1*$^{KG}$ PFC clones. Significant NICD levels are retained on the plasma membrane in *drp1*$^{KG}$ PFC clones marked by CD8GFP relative to nonclonal cells in S6–8 egg chambers (Fig. 2 D). The Notch extracellular domain (NECD) is also retained on the plasma membrane in these clones (Fig. S1 G), confirming that Notch is inactive. In addition, Cut down-regulation, which occurs in response to Notch activation (Sun and Deng, 2007), does not occur in *drp1*$^{KG}$ PFC clones (Fig. 2 E). DRP1-driven mitochondrial fission activity thus acts upstream of Notch activation to drive PFC differentiation.

NICD loss from the membrane (indicative of Notch activation) increases by 28.2% ($n = 30$) in *drp1*$^{KG}$ PFC clones after Marf-1 down-regulation (Fig. 2 F). This suggested that Notch inactivation in *drp1*$^{KG}$ PFC clones is related to mitochondria being highly fused, with mitochondrial fission a prerequisite for Notch receptor activation in the PFCs. Importantly, expression of an activated Notch (N-Act) domain in *drp1*$^{KG}$ PFC clones partially overrides the differentiation block in 53% ($n = 34$) of *drp1*$^{KG}$ PFC clones, resulting in Hnt expression in these clones (Fig. 2 G).

Hoechst (blue) stains nuclei. (D) *drp1*$^{KG}$ PFC clones (lacking UbiGFP) show BrdU incorporation in an S10 egg chamber. (E) *drp1*$^{KG}$ PFC clones (lacking UbiGFP) show pH3-positive cells. Hoechst stains nuclei. (F) Quantification of pH3-positive nuclei in background follicle cells versus *drp1*$^{KG}$ PFC and MBC clones in postmitotic egg chambers. Error bar indicates standard deviation. White lines define the clone boundary, and the dotted lines outline the egg chambers. WT, wild type. Bars, 10 µm.

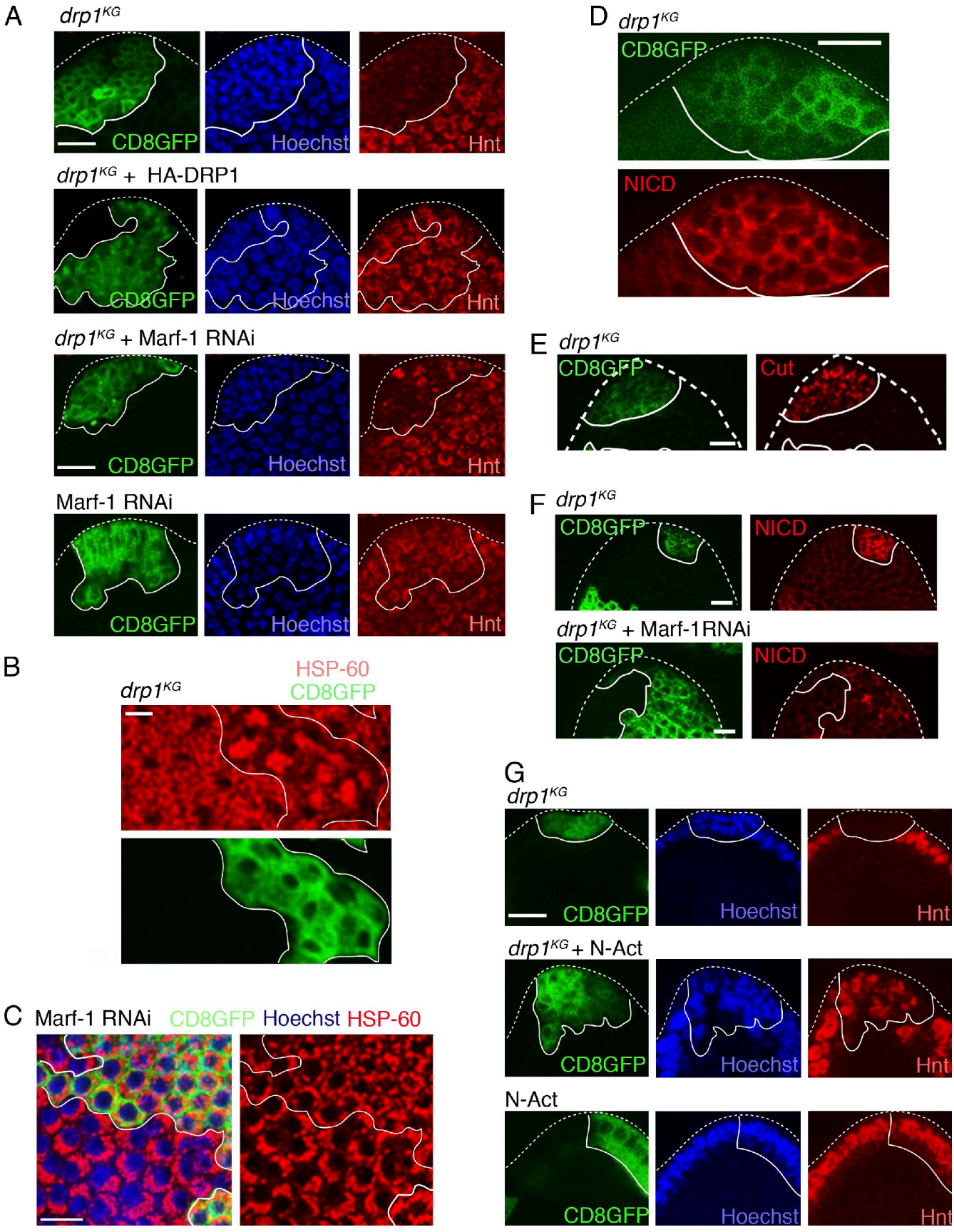
A
drp1KG
CD8GFP
Hoechst
Hnt
drp1KG + HA-DRP1
CD8GFP
Hoechst
Hnt
drp1KG + Marf-1 RNAi
CD8GFP
Hoechst
Hnt
Marf-1 RNAi
CD8GFP
Hoechst
Hnt
B
drp1KG
HSP-60
CD8GFP
C
Marf-1 RNAi
CD8GFP
Hoechst
HSP-60
D
drp1KG
CD8GFP
NICD
E
drp1KG
CD8GFP
Cut
F
drp1KG
CD8GFP
NICD
drp1KG + Marf-1RNAi
CD8GFP
NICD
G
drp1KG
CD8GFP
Hoechst
Hnt
drp1KG + N-Act
CD8GFP
Hoechst
Hnt
N-Act
CD8GFP
Hoechst
Hnt

As this occurs without the fused mitochondrial morphology of *drp1*$^{KG}$ PFC clones changing (Fig. S1 H), the data confirmed that DRP1's role in triggering PFC differentiation is upstream of Notch.

Why is DRP1's role in triggering follicle cell differentiation specific to PFCs? Indeed, *drp1*$^{KG}$ MBC clones show no differentiation block (Fig. 1, C and F; and Fig. S1 A), as Notch activation still occurs in *drp1*$^{KG}$ MBC clones (Fig. S1, I and J). We found higher levels of bound DRP1 in PFCs compared with MBCs after cell permeabilization with digitonin (Fig. S2 A), which may reflect different mitochondrial morphology between PFCs and MBCs. Supporting this, we found in S6–8 ovarioles that mitochondria in PFCs exist as dispersed fragments both apically and basolaterally, whereas mitochondria in MBCs are tightly clustered at the lateral side of the nucleus (Fig. 3, A and B). After S9, no observable differences in mitochondrial morphology are seen (Fig. S2 C).

Fluorescence loss in photobleaching (FLIP) experiments (see Materials and methods) in follicle cells of S6–8 egg chambers revealed that the dispersed mitochondria of PFCs have less matrix continuity relative to the fused mitochondrial cluster of MBCs (Fig. 3, C and D). Furthermore, single-point microirradiation caused a 44% loss in TMRE mitochondrial signal per MBC compared with a 12% loss per PFC (Fig. 3 E). The rapid loss of mitochondrial TMRE signal in MBCs was similar to *drp1*$^{KG}$ clonal cells (Fig. 1 B), with mitochondrial morphology in wild-type MBCs indistinguishable from that of *drp1*$^{KG}$ MBC clones (Fig. S2, D and E). Together, the observed differences in mitochondrial organization and bound DRP1 levels in PFCs and MBCs suggested greater DRP1-driven mitochondrial fission activity occurs in PFCs relative to MBCs. This corroborates our findings in Fig. 1 and Fig. 2 that PFCs, unlike MBCs, differentiate under the influence of DRP1.

PFCs are known to be specified by EGF receptor (EGFR) signaling (Van Buskirk and Schüpbach, 1999). Therefore, we examined mitochondrial morphology upon EGFR signaling modification in postmitotic S6–8 egg chambers. In *egfr*$^{t1}$/*egfr*$^{t1}$ egg chambers (hypomorphic allele of EGFR; González-Reyes et al., 1995), mitochondria in PFCs are primarily clustered to one side of the nucleus, in contrast to those in wild-type or *egfr*$^{t1}$/+ egg chambers, in which mitochondria are dispersed throughout cells (Fig. 3 F). A similar clustering of mitochondria occurs when a dominant-negative (DN) form of EGFR (EGFR-DN) is clonally expressed in the PFC population (Fig. 3 G, clones marked by CD8GFP). Because PFC mitochondria cluster/fuse in the absence of EGFR signaling, the data suggest that EGFR activation in PFCs promotes mitochondria fragmentation in these cells. This could explain why MBCs, which do not receive the EGFR signal, have fused mitochondria. The underlying basis for how EGFR signaling influences mitochondrial dynamics (by altering fission or fusion components) requires further investigation.

Interestingly, PFCs expressing EGFR-DN did not escape differentiation in spite of having clustered mitochondria (Fig. 3 H, EGFR-DN). This may imply that a highly fused mitochondrial cluster may only allow escape from differentiation in the context of activated EGFR signaling. Indeed, EGFR-DN expression in *drp1*$^{KG}$ PFC clones (with fused mitochondria) partially induces differentiation (i.e., Hnt expression) in 40% ($n$ = 38) of the clonal cells compared with no Hnt expression in *drp1*$^{KG}$ PFC clones (Fig. 3 H, *drp1*$^{KG}$ + EGFR-DN and *drp1*$^{KG}$). Expression of an activated form of EGFR (EGFR-Act) did not induce differentiation in *drp1*$^{KG}$ PFC clones (Fig. 2 I). This explains why MBCs, which are not exposed to the EGFR ligand, do not proliferate under DRP1 down-regulation. Thus, cross talk exists between mitochondria and the EGFR signaling pathway in postmitotic PFCs, which helps cells decide whether to differentiate or continue in the mitotic cycle.

We next investigated whether DRP1 activity is important for regulation of cell cycle exit of mitotic follicle cells to allow onset of differentiation. The majority of follicle cells in S1–5 (during which all cells are mitotic) have fragmented mitochondria (Fig. S3, A and B), suggesting that DRP1-dependent fission activity is high. *drp1*$^{KG}$ follicle cell clones introduced into the mitotic follicle cell layer and lacking UbiGFP harbor characteristic mitochondrial clusters (Fig. 4 A). Clones also contain more pH3-positive cells (Fig. 4, B and C) and have qualitatively greater incorporation of BrdU (Fig. S3 C) relative to nonclonal tissue, with Cut expression unaltered (Fig. S3 D). Without DRP1, therefore, S1–5 follicle cells undergo faster mitotic cycling.

To test whether DRP1 activity is necessary for mitotic cells to differentiate, we expressed Marf-1 RNAi to allow unopposed DRP1 activity in S1–5 egg chambers. Strikingly, Marf-1 RNAi expressing follicle cell clones (marked by CD8GFP) show premature expression of Hnt, whereas neighboring nonclonal mitotic follicle cells do not (Fig. 4 D and Fig. S3 E). The effect is not restricted to any stage or region of the mitotic follicle cell layer. The Marf-1 RNAi follicle cell clones exhibit increased mitochondrial mass as assessed by HSP-60 staining (Fig. 4 D) and

Figure 2. **DRP1 down-regulation inhibits Notch-driven differentiation of PFCs in a Marf-1–dependent manner.** (A, top) S8 egg chamber with *drp1*$^{KG}$ PFC clones (CD8GFP label) do not express Hnt, whereas background PFCs (lacking the CD8GFP label) show Hnt labeling. (second row) *drp1*$^{KG}$ PFC clones (CD8GFP label) in constitutive HA-DRP1 background express Hnt. (third row) *drp1*$^{KG}$ + Marf-1 RNAi PFC clones (CD8GFP label) show patches of Hnt-positive cells. (bottom) Marf-1 RNAi clones alone (green) show Hnt labeling. Hoechst stains DNA. (B) Comparison of clustered mitochondrial phenotypes seen in *drp1*$^{KG}$ PFC clones (CD8GFP positive) with fragmented mitochondria (HSP-60) appearing in neighboring nonclonal cells in an S10 egg chamber. (C) Marf-1 RNAi expression (CD8GFP) causes clustered mitochondria (HSP-60) of MBCs in an S8 egg chamber to fragment. Hoechst stains nuclei. See Fig. S1 E for Marf-1 RNAi clones in S10 with the same phenotype. (D) *drp1*$^{KG}$ PFC clones (CD8GFP positive) show massive retention of NICD in the follicle cell plasma membrane of an S8 egg chamber. (E) *drp1*$^{KG}$ PFC clones (CD8GFP positive) show increased Cut labeling compared with the wild-type PFCs in the S8 egg chamber. (F) *drp1*$^{KG}$ + Marf-1 RNAi clones (bottom; CD8GFP positive) show significant loss of membrane NICD in the S8 egg chamber when compared with *drp1*$^{KG}$ clones (top). (G) PFC clones containing activated Notch (N-Act) and *drp1*$^{KG}$ in the S8 egg chamber (middle) show patches of Hnt-positive cells within the multilayer mass of follicle cells, suggesting that N-Act expression can partially override the block in differentiation (i.e., lack of Hnt) seen in *drp1*$^{KG}$ clones (top). (bottom) PFC clones expressing N-Act alone express Hnt and do not overproliferate. The white lines define the clone boundary, and the dotted lines outline the egg chambers. Bars, 10 µm.

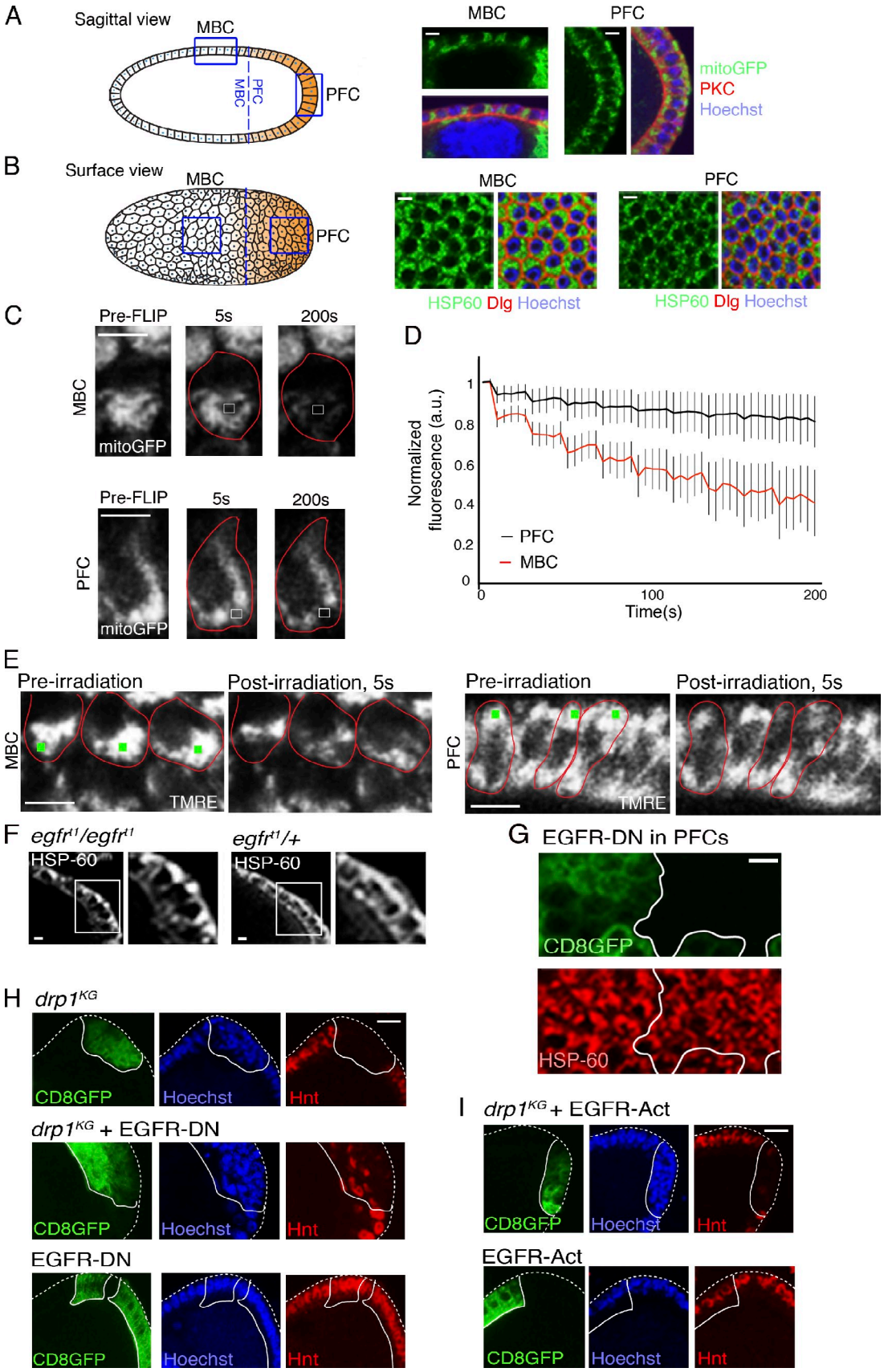


Figure 3. **Mitochondrial morphology differences in PFCs and MBCs established by EGFR signaling.** (A and B, left) Sagittal view (A) and surface view (B) schematic of postmitotic wild-type egg chambers. Blue lines demarcate the boundary between PFC and MBC regions, and orange indicates patterning. (right) Enlarged areas correspond to the boxes in MBC and PFC regions. Low magnification images are shown in Fig. S2 B. Mitochondria were labeled by mito-GFP (A) or HSP-60 (B), nuclei was labeled with Hoechst, PKC marks apical membranes, and Discs large (Dlg) marks lateral membranes of the follicle cells.

MitoTracker loading (Fig. S3 F), similar to that reported previously from mitofusin knockout mice (Chen et al., 2010). Importantly, *drp1*$^{KG}$ follicle cell clones expressing Marf-1 RNAi do not show premature differentiation; Hnt and HSP-60 expression levels are comparable with wild-type cells (Fig. 4 E and Fig. S3 G). Therefore, the premature differentiation of Marf-1 RNAi clones is dependent on DRP1. This indicates that DRP1-driven mitochondrial fission activity is required for mitotic follicle cells to exit the cell cycle and initiate their differentiation regimen.

Because of DRP1's role in differentiation, lack of DRP1 should generate developmental defects. Consistently, DRP1 down-regulation in early follicle cells in the germarium inhibits stalk cell formation, required to separate consecutive egg chambers (Fig. 5 A). The missing stalk cells in egg chambers, encapsulated by early *drp1*$^{KG}$ follicle cell clones, leads to fused egg chambers containing pH3-labeled *drp1*$^{KG}$ clonal cells that lack UbiGFP (Fig. 5 A, arrows; and Video 1). FasIII-enriched polar cells, known to induce stalk cells (López-Schier and St Johnston, 2001), are seen in wild-type ovarioles (Fig. 5 C, left, arrowheads) but are absent in the *drp1*$^{KG}$ clonal follicle cell population (Fig. 5 C, right). Lack of polar cells is not the basis of cell proliferation of *drp1*$^{KG}$ PFCs because FasIII-positive polar cells appear in the surrounding heterozygous tissue (Fig. S3 H). In addition, compound egg chambers with *drp1*$^{KG}$ follicle stem cell clones frequently arise, including egg chambers with 30 nurse cells and two oocytes (Video 2).

Down-regulation of DRP1 also causes developmental defects in the postmitotic follicle cell layer. There, in 22% ($n = 45$) of the cases, *drp1*$^{KG}$ PFC clones fail to trigger migration of the oocyte nucleus toward the anterior (Fig. 5 D, arrows point to nucleus; and Fig. S3 I). The postmitotic stage *drp1*$^{KG}$ phenotypes resemble loss of function of the Hippo–Salvador–Warts pathway (Meignin et al., 2007), which has tumor suppressor effects in higher organisms, including mice (Harvey and Tapon, 2007).

The observed link between cell differentiation and mitochondrial fission state during oogenesis could relate to cyclin E, which controls S-phase entry. Indeed, inhibition of mitochondrial ATP synthesis in a cytochrome oxidase mutant promotes specific degradation of cyclin E (but not other cyclins) and blocks S-phase entry in *Drosophila* (Mandal et al., 2005). In fibroblasts, cyclin E levels increase under conditions of DRP1 inhibition (Mitra et al., 2009). In the *Drosophila* follicle cells studied here, we found that cyclin E levels increase when DRP1 is down-regulated (Fig. S3, J and K) and decrease when Marf-1 is down-regulated (Fig. S3 L). This suggests that DRP1-driven mitochondrial fission activity may cause cell cycle exit by lowering cyclin E levels to allow differentiation.

Our results support a model in which mitochondrial fission/fusion dynamics regulates cell differentiation across the follicle cell layer of the *Drosophila* ovariole (Fig. 5 E). In mitotic stages, increased DRP1-driven mitochondrial fission is required for cell cycle exit as noted in premature DRP1-dependent differentiation of Marf-1 RNAi clones and enhanced proliferation of *drp1*$^{KG}$ clones. During postmitotic transition, activation of EGFR in the posterior region causes mitochondrial fragmentation. This, in turn, permits cell cycle exit and Notch activation, which drives PFC differentiation. In *drp1*$^{KG}$ PFC clones with fused mitochondria, therefore, Notch remains inactive, and cells proliferate. In the main body region, not exposed to the EGFR ligand, postmitotic differentiation and patterning occur in the absence of DRP1. Thus, cell proliferation/differentiation mechanisms have an intimate relationship to mitochondrial morphology and function during follicle layer development.

## Materials and methods

### *Drosophila* strains

All *Drosophila* crosses were performed in standard maize meal agar medium at 25°C. The *drp1*$^{KG03815}$, tubulin (tub)-Gal4, *pointed*-lacZ, EGFRt1, EGFR-DN, and EGFR-Act lines were obtained from the Bloomington Stock Center. The fly strain hsflp; Gal80 flip recombinase target (FRT) 40A/CyO; tub-Gal4, upstream activation sequence (UAS) GFP/TM6 was obtained from N. Grieder (National Institutes of Health, Bethesda, MD). The transgenes carrying N-Act were obtained from S. Artavanis-Tsakonas (Harvard University, Boston, MA). The flies carrying the UAS-*drp1* and UAS-Marf-1 RNAi transgenes were obtained from M. Guo (University of California, Los Angeles, Los Angeles, CA). The UASp-mitochondria (mito)-GFP flies were obtained from R. Cox (Uniformed Services University of Health Sciences, Bethesda, MD). The *drp*$^{KG03815}$ FRT 40A/CyO stock was generated using standard genetic crosses. Flies carrying DRP1-HA were obtained from H. Bellen (Baylor College of Medicine, Houston, TX).

### Generation of follicle cell clones

Homozygous *drp1* mutant clones were generated by flippase (FLP)-FRT–mediated site-specific recombination (Golic and Lindquist, 1989) in the background of heterozygous tissue. Flies containing *drp*$^{KG03815}$ FRT 40A were crossed with hsflp; ubiquitin nls-GFP (ubiGFP) FRT 40A/CyO, hsflp; Gal80 FRT 40A/CyO, or tub-Gal4, UAS-CD8GFP/TM6. 1–3-d adult females carrying the genotype hsflp/+; *drp1* FRT40A/ UbiGFP FRT 40A or hsflp/+; *drp1*$^{KG03815}$ FRT40A/Gal80 FRT40A; tub-Gal4, UAS-CD8GFP/+ were heat pulsed at 38.5 or 37.5°C, respectively, for 15–30 min to generate follicle cell clones. These mosaic females were dissected at 4–6 d for transient clones for estimating pH3-positive cells. For early follicle cell clones, four additional heat shocks were given, two at the third instar larval and two at the pupal stages, at 37°C for 1 h, and dissection was performed after 8–10 d of the adult heat shock. For follicle cell analyses, all the egg chambers with germline clones were ignored. Clones were negatively marked by nuclear GFP carrying an NLS in the control of the ubiquitin promoter or positively marked with CD8GFP with a membrane localization signal. The staging of the egg chambers was performed following Spradling (1993). In addition, internal controls were used for each experiment: pH3 positive for mitotic stages, Cut positive for mitotic stages, NICD down-regulation for postmitotic stages, and Hnt positive for postmitotic stages.

(C) Mitochondrial matrix continuity examined by a FLIP assay (see Materials and methods). MBCs or PFCs expressing mito-GFP (pre-FLIP image) were photobleached repeatedly in the white boxes and monitored for 200 s. Cell boundaries are shown in red. (D) Quantification of FLIP experiment. Total loss of fluorescence was quantified from eight MBCs and eight PFCs from four different egg chambers. Error bars signify standard deviation. (E) Microirradiation (green spots) of TMRE-labeled mitochondria in MBCs versus PFCs in the S8 egg chamber reveals faster loss of TMRE signal in MBCs. Cell boundaries are shown in red. (F) Down-regulation of EGFR in *egfr*$^{1}$/*egfr*$^{1}$ S8 egg chambers causes PFC mitochondrial clustering relative to that in *egfr*$^{1}$/+ chambers. Magnified regions from the boxes are shown on the right. (G) EGFR-DN PFC clones (marked by CD8GFP) in S8 chambers have more tightly clustered mitochondria (labeled with HSP-60) than in surrounding nonclonal cells. (H, middle) *drp1*$^{KG}$ + EGFR-DN PFC clones (CD8GFP label) show patches of Hnt-positive cells. (bottom) EGFR-DN clones alone (CD8GFP label) show Hnt labeling. Hoechst stains DNA. (I, top) *drp1*$^{KG}$ + EGFR-Act PFC clones (CD8GFP label) do not show patches of Hnt-positive cells. (bottom) EGFR-Act clones alone (CD8GFP label) show Hnt labeling. Hoechst stains DNA. The white lines define the clone boundary, and the dotted lines outline the egg chambers. a.u., arbitrary unit. Bars, 5 µm.

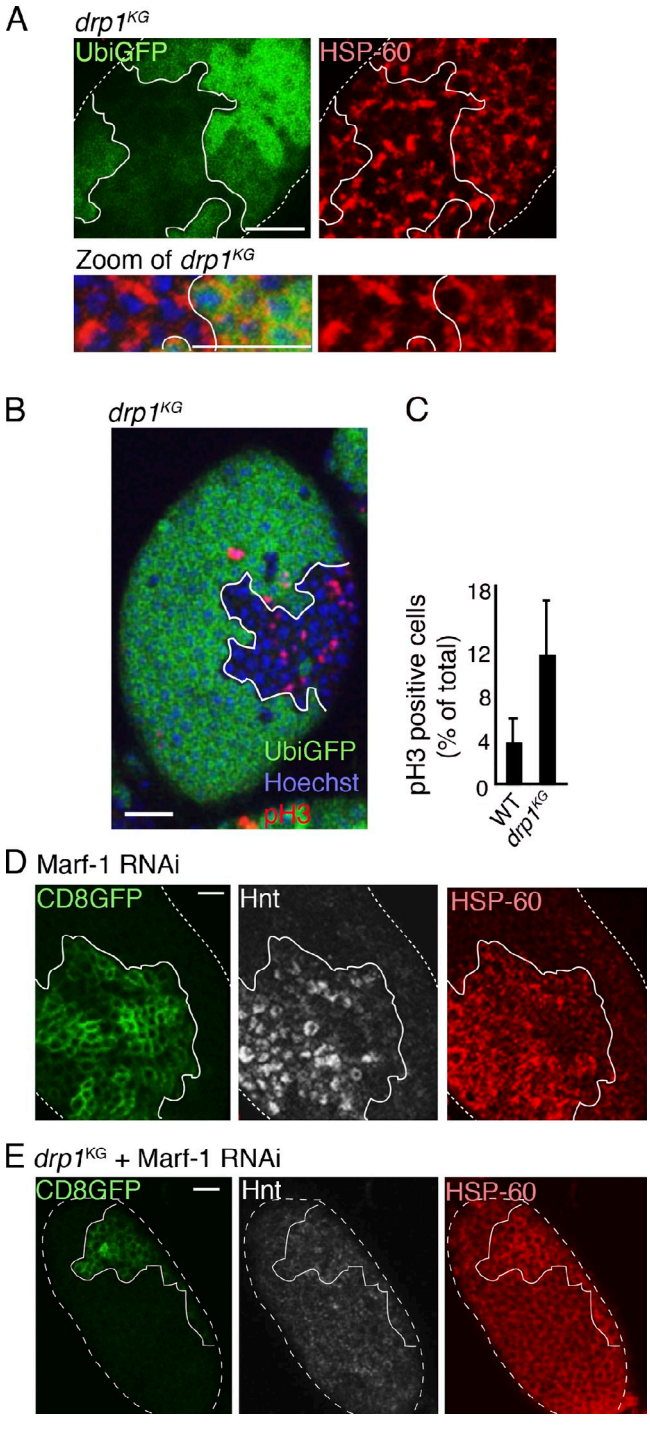


Figure 4. **DRP1 down-regulation inhibits cell cycle exit of mitotic follicle cells.** (A) Mitochondria (HSP-60 labeled) are more clustered in clones of *drp1*$^{KG}$ (lacking UbiGFP) than in nonclonal cells in an S5 mitotic egg chamber. Bottom row shows magnification. Nuclei are stained with Hoechst. (B) Increased pH3 labeling occurs in *drp1*$^{KG}$ clones (lacking UbiGFP) in the S5 egg chamber. (C) Quantification of pH3-positive cells in *drp1*$^{KG}$ clones versus wild-type (WT) background in all mitotic stages. (D) Marf-1 RNAi clones (CD8GFP positive) have increased Hnt and HSP-60 immunolabeling relative to surrounding cells in an S5 mitotic egg chamber. (E) *drp1*$^{KG}$ clones expressing Marf-1 RNAi (CD8GFP positive) show no increase in Hnt or HSP-60 immunolabeling in an S3 mitotic egg chamber. The white lines define the clone boundary, and the dotted lines outline the egg chambers. Bars, 10 µm.

For rescue experiments, transgenes were expressed in the *drp1*$^{KG03815}$ mutant cells using the MARCM (mosaic analysis with a repressible cell marker) technique (Lee and Luo, 1999). Mosaic females were obtained by crossing either control FRT 40A/CyO or mutant *drp1*$^{KG03815}$ FRT 40A/CyO carrying transgenes containing EGRF-Act, EGFR-DN, or N-Act to hsflp; Gal80 FRT 40A/CyO; tub-Gal4, UAS-CD8GFP/TM6 and heat pulsing 1–5-d-old nonbalancer females at 37.5°C for 1 h. The ovaries were dissected at 8–10 d after heat shock. Clones were positively marked by tub-Gal4, UAS-CD8GFP where the GFP labeled the plasma membrane of the clone. The tub-Gal4 was also used to drive the expression of UAS-CD8GFP along with transgenes carrying UAS-Drp1, UAS–N-Act, and UAS-Marf-1 RNAi in the control FRT40A or mutant *drp1*$^{KG03815}$ FRT 40A clone. For complete rescue with HA-DRP1, *drp1*$^{KG}$ clones were generated using heat shock at 38°C for 30 min, whereas partial rescue was observed when bigger clones were generated with 1-h heat shock at the same temperature.

### MitoTracker staining

Ovarioles were dissected in Grace's medium. Live ovarioles were incubated in 250 nM MitoTracker 633 (Invitrogen) for 15 min. Stained ovarioles were rinsed twice in fresh medium and were mounted in water-based mounting medium. Imaging was performed thereafter on a confocal microscope (LSM 510; Carl Zeiss) using a 633-nm laser.

### Immunofluorescence staining

Ovaries were dissected in Grace's insect cell medium at room temperature. For BrdU staining, dissected ovaries were incubated in 50 µM BrdU in Grace's medium for 1 h. Ovaries were washed once with Grace's medium, fixed in 4% PFA, and then acidified and neutralized (Mitra et al., 2009) before immunostaining. For digitonin permeabilization, the dissected ovarioles were incubated with 20 µM digitonin for 5 min and fixed immediately with PFA without any washing step in between and then processed for immunostaining. For all other experiments, dissected tissues were fixed in 4% PFA in PBS for 15 min at room temperature. For immunostaining, fixed tissue was permeabilized in PBS containing 0.3% Triton X-100 (PBST), blocked in PBST containing 2% BSA for 1 h, and treated with primary antibody for 2 h at room temperature or overnight at 4°C. The ovaries were washed with PBST three times for 5 min each. Fluorescent Alexa Fluor (Invitrogen)– or Cy3/Cy5 (Jackson ImmunoResearch Laboratories, Inc.)-conjugated secondary antibodies were added in PBST at room temperature for 1 h. DNA was stained with Hoechst for 10 min. The tissue was washed in PBST three times for 5 min and mounted in Flouromount G (SouthernBiotech). The ovaries were imaged using a laser-scanning confocal microscope (LSM 510). The primary antibodies used were as follows: mouse anti-hnt at 1:100 (Developmental Studies Hybridoma Bank), mouse anti-Cut at 1:100 (Developmental Studies Hybridoma Bank), mouse anti-Fasciclin at 1:100 (Developmental Studies Hybridoma Bank), rabbit anti-pH3 at 1:2,000, mouse anti-NICD at 1:100 (Developmental Studies Hybridoma Bank), mouse anti-NECD at 1:100 (Developmental Studies Hybridoma Bank), rabbit anti-HSP-60 at 1:100 (Stressgen), mouse anti-BrdU at 1:50, and rat anti–Cyclin E at 1:500 (gift from H. Richardson, Peter MacCallum Cancer Center, Melbourne, Australia). The fluorescently coupled secondary antibodies were used at a dilution of 1:1,000.

For quantifying the number of pH3-positive nuclei in different samples, images for an egg chamber were taken at a pinhole setting of 2.5 so that there is no overlap between nuclei in consecutive optical planes. The total numbers of nuclei were estimated from the Hoechst-positive structures in all optical sections per clone. The numbers of pH3-positive structures were estimated as a percentage of the total number of nuclei per clone. A minimum of 30 egg chambers was counted in this method.

Quantification of Hnt-positive clones after expressing various transgenes in *drp1*$^{KG}$ clones included a minimum of 30 egg chambers in each case. Only chambers with clones were counted for this purpose. Clones with Hnt expression in more than five cells were counted as positive. Cell nuclei were identified by Hoechst staining.

Quantification of NICD signal was performed using ImageJ (National Institutes of Health). Maximum intensity projections of two consecutive optical sections were used. Mean pixel intensities of NICD were obtained in the clones and adjacent nonclonal regions. The raw intensity in each case was normalized by the minimum intensity in the region of interest (ROI) to correct for background. The mean intensity of the NICD signal in the clones was normalized to that of the background control PFCs in the same cysts. The results are expressed as the percent decrease in NICD signal in *drp1*$^{KG}$ PFC clones after Marf-1 RNAi expression.

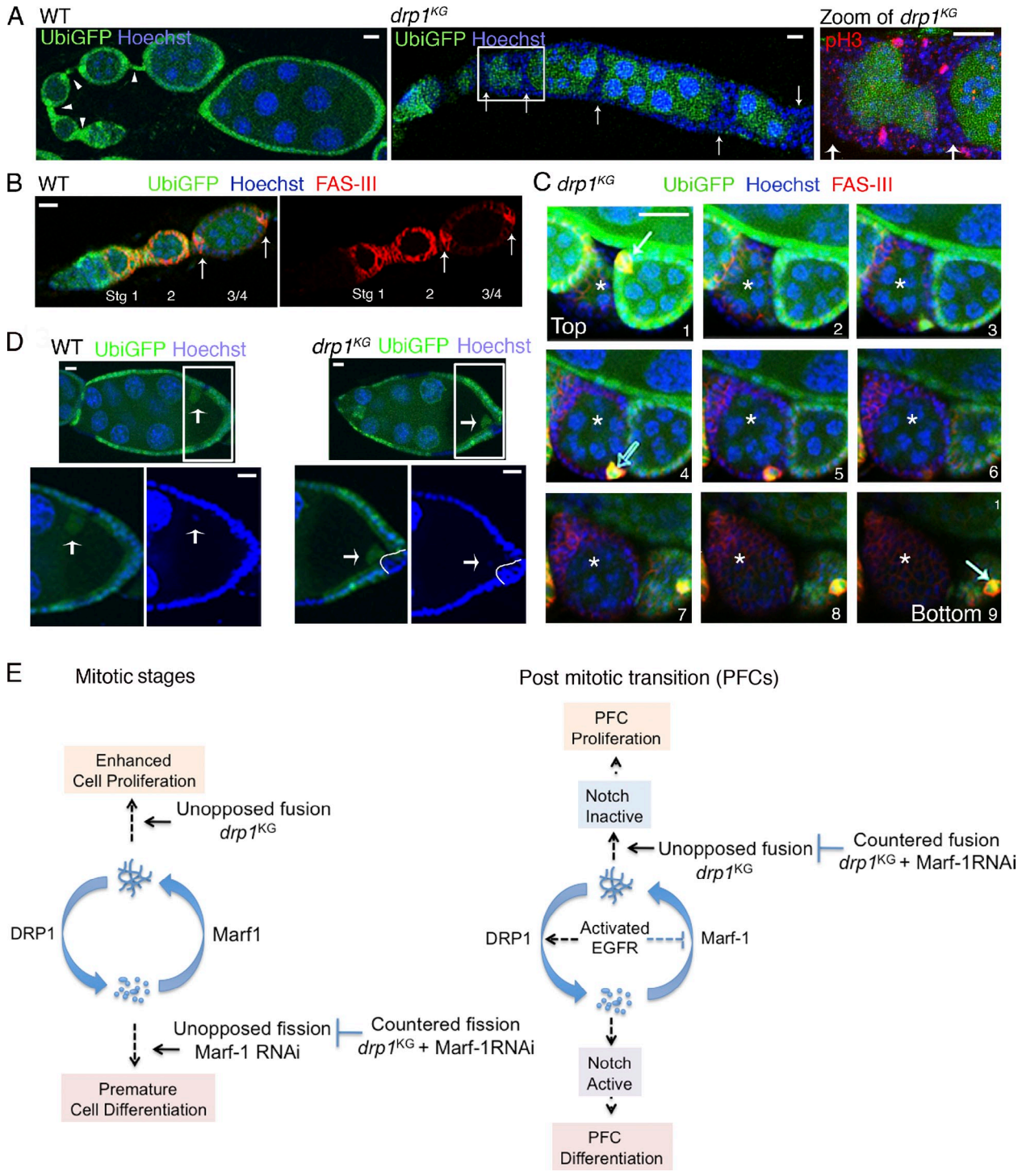


Figure 5. **DRP1 down-regulation causes developmental defects in ovarioles and model for mitochondria's role in cell fate determination.** (A) Down-regulating DRP1 inhibits stalk cell differentiation. Left image shows the wild-type (WT) ovariole. UbiGFP labels wild-type follicle cells, and Hoechst labels DNA. Stalk cells are indicated by arrowheads. Middle image shows ovarioles with *drp1*$^{KG}$ clones (lacking UbiGFP). Arrows indicate regions with no stalk cells. Right image shows presence of the mitotic marker pH3 label in *drp1*$^{KG}$ clonal cells in regions marked by arrows. The boxed region is zoomed in the right. (B) Wild-type egg chambers (with UbiGFP) show FasIII enrichment in polar cells at each termini (arrows) of the egg chamber. Hoechst stains nuclei. (C) Z sectioning through mitotic egg chambers immunostained for FasIII. Sections are arranged in a series, in which numbers represent optical sections from top to bottom. Wild-type chamber (with UbiGFP) has two FasIII-enriched polar cells (arrows in sections 1 and 9). Chamber (asterisks) primarily encapsulated by *drp1*$^{KG}$ clonal follicle cells (no UbiGFP) with only one polar cell pair (open arrow in section 4) and this wild-type FasIII-positive polar cell pair expresses UbiGFP and thus appears yellow. Hoechst stains the nuclei. (D, left) Oocyte nucleus (arrows) after normal migration to the anterior region of oocyte chamber in an S8 wild-type egg chamber. (right) Oocyte nucleus (arrows) in an S8 egg chamber containing *drp1*$^{KG}$ PFC clones (UbiGFP negative) fails to migrate to anterior. Hoechst labels all nuclei, including that of oocyte. Bottom images show magnification of white boxes. White lines define the clone boundary. (E) Model for role of mitochondrial dynamics in determining cell fate in mitotic and postmitotic stages of follicle cell development. Bars, 10 μm.

Quantitation of nuclear repolarization was counted in egg chambers having *drp1*$^{KG}$ clones in the PFC region and compared with egg chambers with no *drp1*$^{KG}$ clones in the PFC regions. Quantitation was performed only from egg chambers at S9 or beyond.

**Live imaging for estimating mitochondrial continuity**

Mitochondrial continuity was estimated by photobleaching and microirradiation experiments (Mitra et al., 2009) on a laser-scanning confocal microscope (LSM 510) using a 63×, 1.0 NA water immersion objective. Experiments were performed in Grace's medium at room temperature (~25°C). Photobleaching experiments were performed with the pUASP-mito-GFP transgene containing the mitochondrial targeting sequence of the human cytochrome oxidase VIII subunit tagged with GFP (Cox and Spradling, 2009). Tub-Gal4 was used to express mito-GFP in the follicle cells during oogenesis. Mito-GFP will target to mitochondria and freely diffuse in the mitochondrial matrix. For live imaging of mitochondria, wild-type ovaries expressing mito-GFP were dissected in Grace's insect cell medium at room temperature. Individual ovarioles were dissected and immediately mounted on a polylysine-coated coverslip in a MatTek chamber. In a FLIP assay, a fixed small ROI (1 × 1 µm) within each cell was repetitively photobleached with a 488-nm laser at 100% power. Image acquisition was performed every 5 s followed by a bleach pulse after every five acquisitions. This protocol will cause the bleaching to spread from the bleached mitochondrial ROI to the mitochondrial regions that maintain matrix continuity with the bleached ROI. Therefore, the FLIP assay measures matrix continuity within mitochondria. Fluorescence intensity was monitored in the sample using an open pinhole for 200 s. Total fluorescence intensity in each cell was quantified using either the proprietary LSM software (Carl Zeiss) or ImageJ. Signal was corrected for background fluorescence and normalized over all photobleaching using signal from an unbleached cell in the same field of view. Data were further normalized against the initial unbleached signal for the respective cell and plotted using Excel (Microsoft). Raw data (without postprocessing) were used for the quantitation. For representative images, brightness/contrast and cropping functions were used with Photoshop (CS2; Adobe).

For microirradiation experiments, wild-type or mosaic ovarioles were dissected in Grace's insect cell medium. They were incubated with 25–50 nM TMRE for 15 min and immediately washed once with medium only before mounting them on polylysine-coated coverslips in a MatTek chamber. The two-photon laser (Chameleon; Coherent, Inc.) was used for microirradiation of a small ROI (0.5 × 0.5 µm) for 250 µs on TMRE-loaded mitochondria in each cell. The 543-nm laser was used for imaging. After microirradiation, fluorescence intensity was monitored for 10 s. Total fluorescence was quantified using the LSM software and expressed as a percentage of the initial signal for each microirradiated cell.

**Online supplemental material**

Fig. S1 shows the effect of mitochondrial fission fusion proteins on mitochondrial morphology and Notch activation. Fig. S2 shows DRP1 abundance in postmitotic follicle cells and mitochondrial morphology in wild-type and in *drp1*$^{KG}$ clones in postmitotic follicle cells. Fig. S3 shows mitochondrial morphology changes between mitotic and postmitotic follicle cells and effects of DRP1 and Marf-1 down-regulation in mitotic and postmitotic stages. Video 1 shows the lack of stalk cell formation with early follicle cell clones of *drp1*$^{KG}$. Video 2 shows that down-regulation of DRP1 in follicle cells generates compound egg chambers. Online supplemental material is available at http://www.jcb.org/cgi/content/full/jcb.201110058/DC1.

We thank Dr. Rachel Cox, Dr. Helena Richardson, Dr. Ming Guo, Dr. Spyros Artavanis-Tsakonas, Dr. Hugo Bellen, and Dr. Nicole Grider for sharing reagents. We are grateful to Dr. Carolyn Ott, Dr. Angelika Rambold, and Dr. Brenda Kostelecy for critical reading of the manuscript and providing helpful comments.

Submitted: 14 October 2011
Accepted: 5 April 2012

## References

Chen, H., S.A. Detmer, A.J. Ewald, E.E. Griffin, S.E. Fraser, and D.C. Chan. 2003. Mitofusins Mfn1 and Mfn2 coordinately regulate mitochondrial fusion and are essential for embryonic development. *J. Cell Biol.* 160:189–200. http://dx.doi.org/10.1083/jcb.200211046

Chen, H., M. Vermulst, Y.E. Wang, A. Chomyn, T.A. Prolla, J.M. McCaffery, and D.C. Chan. 2010. Mitochondrial fusion is required for mtDNA stability in skeletal muscle and tolerance of mtDNA mutations. *Cell.* 141:280–289. http://dx.doi.org/10.1016/j.cell.2010.02.026

Cox, R.T., and A.C. Spradling. 2009. Clueless, a conserved *Drosophila* gene required for mitochondrial subcellular localization, interacts genetically with parkin. *Dis Model Mech.* 2:490–499. http://dx.doi.org/10.1242/dmm.002378

de Cuevas, M., M.A. Lilly, and A.C. Spradling. 1997. Germline cyst formation in *Drosophila*. *Annu. Rev. Genet.* 31:405–428. http://dx.doi.org/10.1146/annurev.genet.31.1.405

Deng, H., M.W. Dodson, H. Huang, and M. Guo. 2008. The Parkinson's disease genes pink1 and parkin promote mitochondrial fission and/or inhibit fusion in *Drosophila*. *Proc. Natl. Acad. Sci. USA.* 105:14503–14508. http://dx.doi.org/10.1073/pnas.0803998105

Frank, S., B. Gaume, E.S. Bergmann-Leitner, W.W. Leitner, E.G. Robert, F. Catez, C.L. Smith, and R.J. Youle. 2001. The role of dynamin-related protein 1, a mediator of mitochondrial fission, in apoptosis. *Dev. Cell.* 1:515–525. http://dx.doi.org/10.1016/S1534-5807(01)00055-7

Golic, K.G., and S. Lindquist. 1989. The FLP recombinase of yeast catalyzes site-specific recombination in the *Drosophila* genome. *Cell.* 59:499–509. http://dx.doi.org/10.1016/0092-8674(89)90033-0

Gomes, L.C., G. Di Benedetto, and L. Scorrano. 2011. During autophagy mitochondria elongate, are spared from degradation and sustain cell viability. *Nat. Cell Biol.* 13:589–598. http://dx.doi.org/10.1038/ncb2220

González-Reyes, A., H. Elliott, and D. St Johnston. 1995. Polarization of both major body axes in *Drosophila* by gurken-torpedo signalling. *Nature.* 375:654–658. http://dx.doi.org/10.1038/375654a0

Goyal, G., B. Fell, A. Sarin, R.J. Youle, and V. Sriram. 2007. Role of mitochondrial remodeling in programmed cell death in *Drosophila melanogaster*. *Dev. Cell.* 12:807–816. http://dx.doi.org/10.1016/j.devcel.2007.02.002

Harvey, K., and N. Tapon. 2007. The Salvador-Warts-Hippo pathway - an emerging tumour-suppressor network. *Nat. Rev. Cancer.* 7:182–191. http://dx.doi.org/10.1038/nrc2070

Horn, S.R., M.J. Thomenius, E.S. Johnson, C.D. Freel, J.Q. Wu, J.L. Coloff, C.S. Yang, W. Tang, J. An, O.R. Ilkayeva, et al. 2011. Regulation of mitochondrial morphology by APC/CCdh1-mediated control of Drp1 stability. *Mol. Biol. Cell.* 22:1207–1216. http://dx.doi.org/10.1091/mbc.E10-07-0567

Ingerman, E., E.M. Perkins, M. Marino, J.A. Mears, J.M. McCaffery, J.E. Hinshaw, and J. Nunnari. 2005. Dnm1 forms spirals that are structurally tailored to fit mitochondria. *J. Cell Biol.* 170:1021–1027. http://dx.doi.org/10.1083/jcb.200506078

Ishihara, N., M. Nomura, A. Jofuku, H. Kato, S.O. Suzuki, K. Masuda, H. Otera, Y. Nakanishi, I. Nonaka, Y. Goto, et al. 2009. Mitochondrial fission factor Drp1 is essential for embryonic development and synapse formation in mice. *Nat. Cell Biol.* 11:958–966. http://dx.doi.org/10.1038/ncb1907

Jasper, H., V. Benes, A. Atzberger, S. Sauer, W. Ansorge, and D. Bohmann. 2002. A genomic switch at the transition from cell proliferation to terminal differentiation in the *Drosophila* eye. *Dev. Cell.* 3:511–521. http://dx.doi.org/10.1016/S1534-5807(02)00297-6

Lee, T., and L. Luo. 1999. Mosaic analysis with a repressible cell marker for studies of gene function in neuronal morphogenesis. *Neuron.* 22:451–461. http://dx.doi.org/10.1016/S0896-6273(00)80701-1

López-Schier, H., and D. St Johnston. 2001. Delta signaling from the germ line controls the proliferation and differentiation of the somatic follicle cells during *Drosophila* oogenesis. *Genes Dev.* 15:1393–1405. http://dx.doi.org/10.1101/gad.200901

Mandal, S., P. Guptan, E. Owusu-Ansah, and U. Banerjee. 2005. Mitochondrial regulation of cell cycle progression during development as revealed by the tenured mutation in *Drosophila*. *Dev. Cell.* 9:843–854. http://dx.doi.org/10.1016/j.devcel.2005.11.006

Meignin, C., I. Alvarez-Garcia, I. Davis, and I.M. Palacios. 2007. The salvador-warts-hippo pathway is required for epithelial proliferation and axis specification in *Drosophila*. *Curr. Biol.* 17:1871–1878. http://dx.doi.org/10.1016/j.cub.2007.09.062

Mitra, K., C. Wunder, B. Roysam, G. Lin, and J. Lippincott-Schwartz. 2009. A hyperfused mitochondrial state achieved at G1-S regulates cyclin E buildup and entry into S phase. *Proc. Natl. Acad. Sci. USA.* 106:11960–11965. http://dx.doi.org/10.1073/pnas.0904875106

Rambold, A.S., B. Kostelecky, N. Elia, and J. Lippincott-Schwartz. 2011. Tubular network formation protects mitochondria from autophagosomal degradation during nutrient starvation. *Proc. Natl. Acad. Sci. USA.* 108:10190–10195. http://dx.doi.org/10.1073/pnas.1107402108

Roth, S. 2001. *Drosophila* oogenesis: coordinating germ line and soma. *Curr. Biol.* 11:R779–R781. http://dx.doi.org/10.1016/S0960-9822(01)00469-9

Ruohola, H., K.A. Bremer, D. Baker, J.R. Swedlow, L.Y. Jan, and Y.N. Jan. 1991. Role of neurogenic genes in establishment of follicle cell fate and oocyte polarity during oogenesis in *Drosophila*. *Cell.* 66:433–449. http://dx.doi.org/10.1016/0092-8674(81)90008-8

Spradling, A.C. 1993. Developmental genetics of oogenesis. *In* The Development of *Drosophila melanogaster.* Vol. 1. M. Bate and A. Martinez Arias, editors. Cold Spring Harbor Laboratory Press, Plainview, NY. 1–70.

Sun, J., and W.M. Deng. 2007. Hindsight mediates the role of notch in suppressing hedgehog signaling and cell proliferation. *Dev. Cell*. 12:431–442. http://dx.doi.org/10.1016/j.devcel.2007.02.003

Taguchi, N., N. Ishihara, A. Jofuku, T. Oka, and K. Mihara. 2007. Mitotic phosphorylation of dynamin-related GTPase Drp1 participates in mitochondrial fission. *J. Biol. Chem.* 282:11521–11529. http://dx.doi.org/10.1074/jbc.M607279200

Twig, G., A. Elorza, A.J. Molina, H. Mohamed, J.D. Wikstrom, G. Walzer, L. Stiles, S.E. Haigh, S. Katz, G. Las, et al. 2008. Fission and selective fusion govern mitochondrial segregation and elimination by autophagy. *EMBO J.* 27:433–446. http://dx.doi.org/10.1038/sj.emboj.7601963

Van Buskirk, C., and T. Schüpbach. 1999. Versatility in signalling: multiple responses to EGF receptor activation during *Drosophila* oogenesis. *Trends Cell Biol.* 9:1–4. http://dx.doi.org/10.1016/S0962-8924(98)01413-5

van Eeden, F., and D. St Johnston. 1999. The polarisation of the anterior-posterior and dorsal-ventral axes during *Drosophila* oogenesis. *Curr. Opin. Genet. Dev.* 9:396–404. http://dx.doi.org/10.1016/S0959-437X(99)80060-4